ACS Photonics

pubs.acs.org/journal/apchd5 Article

Third-Order Optical Nonlinearity of Three-Dimensional Massless Dirac Fermions

J. L. Cheng,* J. E. Sipe, and S. W. Wu

Cite This: *ACS Photonics* 2020, 7, 2515−2526 Read Online

ACCESS | Metrics & More | Article Recommendations

ABSTRACT: We present analytic expressions for the electronic contributions to the linear conductivity $\sigma^{(1)}_{3d}(\omega)$ and the third-order optical conductivity $\sigma^{(3)}_{3d}(\omega_1, \omega_2, \omega_3)$ of three-dimensional massless Dirac Fermions, the quasi-particles relevant for the low energy excitation of topological Dirac and Weyl semimetals. Although there is no gap for massless Dirac Fermions, a finite chemical potential μ can lead to an effective gap parameter, which plays an important role in the qualitative features of interband optical transitions. For gapless linear dispersion in three dimensions, the imaginary part of the linear conductivity diverges as a logarithmic function of the cutoff energy, while the real part is linear, with a photon frequency ω as $\hbar\omega > 2|\mu|$. The third-order conductivity exhibits features very similar to those of two-dimensional Dirac Fermions, that is, graphene, but with the amplitude for a single Dirac cone generally 2 orders of magnitude smaller in three dimensions than in two dimensions. There are many resonances associated with the chemical-potential-induced gap parameters and divergences associated with the intraband transitions. The details of the third-order conductivity are discussed for third-harmonic generation, the Kerr effect and two-photon carrier injection, parametric frequency conversion, and two-color coherent current injection. Although the expressions we derive are limited to the clean limit at zero temperature, the generalization to include phenomenological relaxation processes at finite temperature is straightforward and is presented. In contrast with 2D materials, the bulk nature of materials that host three-dimensional Dirac Fermions allows for the possibility of enhancing nonlinear signals by tuning the sample thickness; thus, broad applications of such materials in nonlinear photonic devices can be envisioned.

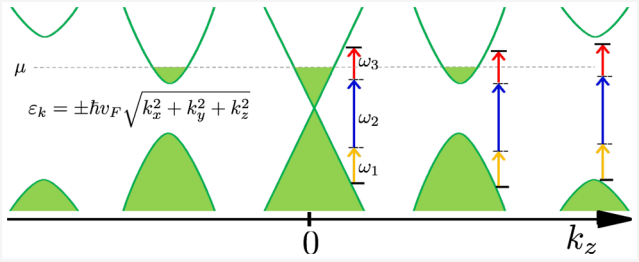

KEYWORDS: *Dirac semimetals, gapped graphene, third-harmonic generation, Kerr effect, parametric frequency conversion, two-color coherent current injection, length gauge*

Two-dimensional (2D), massless Dirac Fermions (DFs) have been investigated extensively in condensed matter systems since their first experimental realization in graphene, and their properties are significantly different than those of Fermions in the more usual parabolic bands.[1,2] Their attractive optical properties[3] include broadband linear optical absorption and the ability to use the chemical potential to tune both plasmon resonances and an extremely strong nonlinear optical response.[4] The strong nonlinear response makes graphene a potential candidate for integration in photonic devices[5−7] as a source of nonlinear functionality, and it has been the focus of a large number of experimental[8,9] and theoretical[10−18] studies over the past decade. Experiments have explored different nonlinear phenomena, including third-harmonic generation (THG), the Kerr effect and two-photon carrier injection, parametric frequency conversion (PFC), and two-color coherent current injection (CCI); the corresponding nonlinear coefficients have been extracted for different photon energies and chemical potentials. Theoretical studies have been mainly at the level of independent particle approximation and have presented perturbative expressions and numerical simulations. Recently, many-body effects[19−21] have been shown to play a significant role in the nonlinear optical response. And in the development of theories of topological materials, 2D massless DFs have been shown to determine the properties of the low-energy excitation of surface states of topological insulators, despite the small energy range over which the linear dispersion approximation is valid.

In a two-band model for 2D DFs, a mass can be introduced. The resulting dispersion relation can be realized around the band edge of the gapped graphene or around the band edge of a monolayer of BN or MoS_2, and in other 2D materials. The optical nonlinearities of 2D massive DFs have also been investigated both experimentally and theoretically. Jafari[22]

Received: May 21, 2020
Published: July 27, 2020

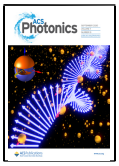

https://dx.doi.org/10.1021/acsphotonics.0c00836
ACS Photonics 2020, 7, 2515−2526

presented a theory for THG using a Feynman diagrammatic technique, describing the light−matter interaction in the framework of a vector potential. However, in the limit of vanishing mass, the result does not converge to the results of other studies.[11] Cheng et al. investigated various nonlinear effects both by numerically solving the equations of motion[13] and by approximation from the results of gapped graphene under a perpendicular magnetic field.[23] Recently, we derived analytic expressions for the third-order conductivities of gapped graphene[24] at general frequencies, following earlier work on graphene.[12]

There have also been a host of recent studies focused on the prediction and discovery of three-dimensional (3D) Dirac and Weyl semimetals,[25−32] where the low-energy excitations can be described by DFs with a 3D wave vector. As an analogue of 2D massless DFs, 3D massless DFs[32] possess gapless linear dispersion and an interesting band topology around the Dirac point, which leads to extraordinary optical properties. As well, the chiral anomaly in Weyl semimetals can be probed with the presence of both the electric field and magnetic field.[33] The nonlinear optical properties of 3D massless DFs have also attracted attention.[34−40] Experimentally, huge nonlinear optical coefficients[41] have been observed, although probably at frequencies much higher than those at which the linear dispersion approximation is valid. There are interesting recent theoretical predictions[42−44] for the Kerr effect and THG, both within the framework of the Boltzmann equation and in a treatment, including intraband and interband transitions. In these studies, the focus was on frequencies in the terahertz regime, and possible applications in terahertz plasmonics have been investigated,[45] including a promising proposal for extinction modulations.[42] However, the light−matter interaction was described in a velocity gauge, and additional care may be required to confirm that no nonphysical divergences have been induced by band truncation; a treatment based on the length gauge,[46,47] where such difficulties are not present, is clearly in order. Further, in order to extend the application of these materials to various nonlinear optical scenarios, it would be helpful to understand the general frequency dependence of the third-order conductivity, especially in a comparison with that of graphene; this has not yet been done.

In this work, we derive analytic expressions for linear and third order optical conductivities of 3D massless DFs. Our strategy is based on employing earlier results found for the linear and nonlinear optical response of gapped graphene. In fact, we show that the response coefficients for 3D massless DFs can be written as an integral over the results for gapped graphene with different gaps. Our treatment includes the intraband and interband optical transitions in a framework where the light−matter interaction is described in the length gauge. Our expressions for the third-order conductivities describe a general input frequency dependence for the clean limit at zero temperature. After analyzing the structures of the conductivities, we discuss in detail the coefficients for THG, the Kerr effect and two-photon carrier injection, PFC, and two-color CCI. To better understand the physics of the nonlinear processes, comparisons with that of graphene are made. Our expressions can be used to generate input nonlinear parameters for evaluating the performace of various photonic devices, including some optical modulators[42] and frequency generation devices.[48]

We organized the paper as follows: in "Models", we summarize the symmetries of the frequency dependence of the linear and nonlinear conductivities of 2D massive DFs. In the next section, we describe how to construct the conductivity of 3D massless DFs from the conductivity of 2D massive DFs and present the analytic expressions for linear conductivity and third-order conductivity; in "Results", we discuss the details of the conductivities for different optical phenomena, including the linear optical response, THG, the Kerr effect and two-photon carrier injection, PFC, and two-color CCI; in "Conclusion and Discussion" we discuss and conclude, indicating how the extension of our results to include finite temperature and a phenomenological description of relaxation processes can easily be implemented.

MODELS

Conductivities for 2D Dirac Fermions. Two-dimensional massive DFs in one Dirac cone can be described by the Hamiltonian

$$H_{2d}(\boldsymbol{\kappa}, \Delta) = \hbar v_F \boldsymbol{\kappa}\cdot\boldsymbol{\sigma} + \Delta\sigma_z \tag{1}$$

where v_F is the Fermi velocity, $\boldsymbol{\sigma} = \sigma_x\hat{\boldsymbol{x}} + \sigma_y\hat{\boldsymbol{y}} + \sigma_z\hat{\boldsymbol{z}}$ has its components as Pauli matrices, $\boldsymbol{\kappa} = \kappa_x\hat{\boldsymbol{x}} + \kappa_y\hat{\boldsymbol{y}}$ is a 2D wave vector, and Δ is a mass parameter to give a gap $2|\Delta|$ at the Dirac point. Depending on the material, there can exist multiple Dirac cones, and for different materials, the model Hamiltonian can take in different forms. For example, the low energy excitations of gapped graphene are described by the Hamiltonian

$$H_{gg;\tau}(\boldsymbol{\kappa}, \Delta) = \hbar v_F(\tau\kappa_y\sigma_x - \kappa_x\sigma_y) + \Delta\sigma_z \tag{2}$$

where $\tau = \pm$ is a valley index for two different Dirac cones.

For such Hamiltonians, we consider the linear optical conductivity tensor $\sigma^{(1);da}(\omega)$ and third order optical conductivity tensor $\sigma^{(3);dabc}(\omega_1, \omega_2, \omega_3)$, where the Roman letters d, a, b, and c refer to the Cartesian directions, and ω and ω_i refer to the optical frequencies. The second-order response vanishes in the dipole approximation, as we discuss below. The results of gapped graphene have been given earlier[24] and will be summarized in the following.

Symmetry Properties of Conductivities for Two-Dimensional Massive Dirac Fermions. We denote the conductivities for a 2D Dirac cone by $\sigma_{2d}^{(1);da}(\omega)$ and $\sigma_{2d}^{(3);dabc}(\omega_1, \omega_2, \omega_3)$. The Hamiltonian $H_{2d}(\boldsymbol{\kappa}, \Delta)$ satisfies the rotational symmetry condition

$$U_\theta H_{2d}(R_\theta\boldsymbol{\kappa}, \Delta)U_\theta^\dagger = H_{2d}(\boldsymbol{\kappa}, \Delta) \tag{3}$$

where θ is a rotation angle about the z axis, $U_\theta = \cos\theta/2 - i\sin\theta/2\sigma_z$ is a unitary transformation acting on the spinors, and $R_\theta = \begin{pmatrix} \cos\theta & \sin\theta \\ -\sin\theta & \cos\theta \end{pmatrix}$ is rotation operation acting on $\boldsymbol{\kappa}$. The rotational symmetry determines that the linear conductivity includes only two independent components, that is, the diagonal component $\sigma_{2d}^{(1);xx}$ and the off-diagonal component $\sigma_{2d}^{(1);xy}$. The other nonzero components can be found from

$$\sigma_{2d}^{(1);xx} = \sigma_{2d}^{(1);yy}, \quad \sigma_{2d}^{(1);xy} = -\sigma_{2d}^{(1);yx} \tag{4}$$

The off-diagonal components are nonzero because the Berry curvature at the Dirac point behaves as the vector potential of a magnetic monopole, and can contribute to a Hall conductivity. For the third-order conductivity, there are in all six independent nonzero components, which can be taken to be

https://dx.doi.org/10.1021/acsphotonics.0c00836
ACS Photonics 2020, 7, 2515−2526

$\sigma_{2d}^{(3);xxyy}$, $\sigma_{2d}^{(3);xyxy}$, $\sigma_{2d}^{(3);xyyx}$, $\sigma_{2d}^{(3);yxyy}$, $\sigma_{2d}^{(3);yyxy}$, and $\sigma_{2d}^{(3);yyyx}$. The other nonzero components are then given by

$$\sigma_{2d}^{(3);xxxx} = \sigma_{2d}^{(3);xxyy} + \sigma_{2d}^{(3);xyxy} + \sigma_{2d}^{(3);xyyx} \tag{5}$$

$$\sigma_{2d}^{(3);yxxx} = \sigma_{2d}^{(3);yxyy} + \sigma_{2d}^{(3);yyxy} + \sigma_{2d}^{(3);yyyx} \tag{6}$$

and

$$\sigma_{2d}^{(3);xxxx} = \sigma_{2d}^{(3);yyyy}, \quad \sigma_{2d}^{(3);yxxx} = -\sigma_{2d}^{(3);xyyy} \tag{7}$$

$$\sigma_{2d}^{(3);xxyy} = \sigma_{2d}^{(3);yyxx}, \quad \sigma_{2d}^{(3);yxyy} = -\sigma_{2d}^{(3);xyxx} \tag{8}$$

$$\sigma_{2d}^{(3);xyxy} = \sigma_{2d}^{(3);yxyx}, \quad \sigma_{2d}^{(3);yyxy} = -\sigma_{2d}^{(3);xxyx} \tag{9}$$

$$\sigma_{2d}^{(3);xyyx} = \sigma_{2d}^{(3);yxxy}, \quad \sigma_{2d}^{(3);yyyx} = -\sigma_{2d}^{(3);xxxy} \tag{10}$$

For a single Dirac cone, the independent components $\sigma_{2d}^{(1);xy}$, $\sigma_{2d}^{(3);yxyy}$, $\sigma_{2d}^{(3);yyxy}$, and $\sigma_{2d}^{(3);yyyx}$ are antisymmetric with respect to $\{x \leftrightarrow y\}$, while the others, $\sigma_{2d}^{(1);xx}$, $\sigma_{2d}^{(3);xxyy}$, $\sigma_{2d}^{(3);xyxy}$, and $\sigma_{2d}^{(3);xyyx}$ are symmetric; we refer to these two different classes of tensor components as "antisymmetric" and "symmetric" components, respectively. Due to inversion symmetry

$$\sigma_z H_{2d}(-\boldsymbol{\kappa}, \Delta)\sigma_z = H_{2d}(\boldsymbol{\kappa}, \Delta) \tag{11}$$

and there is no second order response in the dipole approximation.

For 2D DFs, the sign of the mass parameter determines the chirality, and the two different possibilities are connected through

$$U_m H_{2d}(R_m\boldsymbol{\kappa}, \Delta)U_m^{\dagger} = H_{2d}(\boldsymbol{\kappa}, -\Delta) \tag{12}$$

with $U_m = i/\sqrt{2}(\sigma_x - \sigma_y)$ and $R_i = \begin{pmatrix} 0 & -1 \\ -1 & 0 \end{pmatrix}$. This relation gives $\sigma_{2d}^{(n);dab\cdots}(-\Delta) = \sigma_{2d}^{(n);\bar{d}\,\bar{a}\,\bar{b}\cdots}(\Delta)$, where the bar of a Roman letter means $\bar{d} = y, x$ for $d = x, y$. Furthermore, utilizing the consequences of rotational symmetry, we find that all symmetric (antisymmetric) components are even (odd) functions of Δ.

Conductivities of Gapped Graphene. We denote the conductivities that follow from the Hamiltonian $H_{gg;\tau}$ by $\sigma_{gg;\tau}^{(1);da}(\omega)$ and $\sigma_{gg;\tau}^{(3);dabc}(\omega_1, \omega_2, \omega_3)$. In the τ valley ($\tau = \pm 1$), the Hamiltonian connects to $H_{2d}(\boldsymbol{\kappa}, \Delta)$ through

$$H_{gg;\tau}(\boldsymbol{\kappa}, \Delta) = H_{2d}(R_\tau\boldsymbol{\kappa}, \Delta) \tag{13}$$

with an orthogonal matrix $R_\tau = \begin{pmatrix} 0 & \tau \\ -1 & 0 \end{pmatrix}$. From eq 13, the symmetric components satisfy $\sigma_{gg;\tau}^{(n);da\cdots}(\Delta) = \sigma_{2d}^{(n);\bar{d}\bar{a}\cdots}(\Delta)$, and antisymmetric components satisfy $\sigma_{gg;\tau}^{(n);da\cdots}(\Delta) = \tau\sigma_{2d}^{(1);\bar{d}\bar{a}\cdots}(\Delta)$. Therefore, for gapped graphene only the symmetric components survive, and they are

$$\sigma_{gg}^{(1);xx}(\omega) = 2\sum_{\tau}\sigma_{gg;\tau}^{(1);xx}(\omega) = 4\sigma_{2d}^{(1);xx}(\omega) \tag{14}$$

where the prefactor 2 comes from the spin degeneracy in gapped graphene. Similarly, the third-order conductivities are

$$\sigma_{gg}^{(3);dabc}(\omega_1, \omega_2, \omega_3) = 4\sigma_{2d}^{(3);dabc}(\omega_1, \omega_2, \omega_3) \tag{15}$$

for $dabc = xxyy$, $xyxy$, and $xyyx$.

The optical conductivities of gapped graphene under the linear dispersion approximation have been studied, and analytical expressions for them have been obtained.[24] For later use, we list the expressions in the clean limit. The linear conductivity is given by

$$\sigma_{gg}^{(1);xx}(\omega) = \frac{i\sigma_0}{\pi}\left[\frac{4E_c}{\hbar\omega} - \frac{4\Delta^2 + (\hbar\omega)^2}{(\hbar\omega)^2}\mathcal{G}(E_c; \hbar\omega)\right] \tag{16}$$

Here $\sigma_0 = e^2/4\hbar$ is a universal conductivity, $E_c = \max\{|\Delta|,|\mu|\}$ is an effective gap parameter, and

$$\mathcal{G}(E_c; \hbar\omega) = \ln\left|\frac{\hbar\omega + 2E_c}{\hbar\omega - 2E_c}\right| + i\pi\theta(|\hbar\omega| - 2E_c) \tag{17}$$

with $\theta(x)$ being the usual step function. For the third order conductivity, the cyclic permutation symmetry on $\{a\omega_1, b\omega_2, c\omega_3\}$ of $\sigma_{gg}^{(3);dabc}(\omega_1, \omega_2, \omega_3)$ gives

$$\sigma_{gg}^{(3);xxyy}(\omega_1, \omega_2, \omega_3) = \sigma_{gg}^{(3);xyxy}(\omega_2, \omega_1, \omega_3) = \sigma_{gg}^{(3);xyyx}(\omega_2, \omega_3, \omega_1) \tag{18}$$

The third order conductivity is then

$$\begin{aligned}(i\sigma_3)^{-1}\sigma_{gg}^{(3);xxyy}&(\omega_1, \omega_2, \omega_3)\\ &= F_1(\Delta; \hbar\omega_1, \hbar\omega_2, \hbar\omega_3)\mathcal{G}(E_c; \hbar(\omega_1 + \omega_2 + \omega_3))\\ &\quad + F_2(\Delta; \hbar\omega_1, \hbar\omega_2, \hbar\omega_3)\mathcal{G}(E_c; \hbar(\omega_2 + \omega_3))\\ &\quad + F_3(\Delta; \hbar\omega_1, \hbar\omega_2, \hbar\omega_3)\mathcal{G}(E_c; \hbar(\omega_1 + \omega_3))\\ &\quad + F_3(\Delta; \hbar\omega_1, \hbar\omega_3, \hbar\omega_2)\mathcal{G}(E_c; \hbar(\omega_1 + \omega_2))\\ &\quad + F_4(\Delta; \hbar\omega_1, \hbar\omega_2, \hbar\omega_3)\mathcal{G}(E_c; \hbar\omega_1)\\ &\quad + F_5(\Delta; \hbar\omega_1, \hbar\omega_2, \hbar\omega_3)\mathcal{G}(E_c; \hbar\omega_2)\\ &\quad + F_5(\Delta; \hbar\omega_1, \hbar\omega_3, \hbar\omega_2)\mathcal{G}(E_c; \hbar\omega_3).\end{aligned} \tag{19}$$

with $\sigma_3 = \sigma_0(\hbar v_F e)^2/\pi$. The coefficients F_i are given by

$$F_i(\Delta; \epsilon_1, \epsilon_2, \epsilon_3) = \mathcal{F}_{i0}(\epsilon_1, \epsilon_2, \epsilon_3) + \Delta^2\mathcal{F}_{i2}(\epsilon_1, \epsilon_2, \epsilon_3) + \Delta^4\mathcal{F}_{i4}(\epsilon_1, \epsilon_2, \epsilon_3) \tag{20}$$

All the expressions of $\mathcal{F}_{ij}$ are given in "Methods". By setting $\Delta = 0$, we get the third-order nonlinear conductivity for graphene as

$$\sigma_{gh}^{(3);xxyy}(\omega_1, \omega_2, \omega_3) = \sigma_{gg}^{(3);xxyy}(\omega_1, \omega_2, \omega_3)\Big|_{\Delta=0} \tag{21}$$

We briefly discuss the asymptotic expression of these conductivities as $\Delta \to \infty$. In that limit, $E_c = \max\{|\Delta|,|\mu|\} = \Delta$, and all involved photon energies satisfy $\hbar\omega_i/E_c \to 0$. As $\Delta \to \infty$, a direct expansion in the small quantities $\hbar\omega_i/\Delta$ gives

$$\sigma_{gg}^{(1);xx}(\omega) \to -i\sigma_0\frac{4\hbar\omega}{3\pi\Delta} \tag{22}$$

$$\sigma_{gg}^{(3);xxyy}(\omega_1, \omega_2, \omega_3) \to -i\sigma_3\frac{2\hbar(\omega_1 + \omega_2 + \omega_3)}{45\Delta^5} \tag{23}$$

The effective gap parameters E_c in eq 19 appear only in functions of $\mathcal{G}$, which determine possible resonances related to the interband transitions. Considering the photon energies involved in these functions, we note that the resonances can be associated with one-photon, two-photon, and three-photon processes. Both the one-photon and three-photon related resonances are similar to that of the linear conductivity, while the two-photon related resonance shows a different behavior. Since $F_2(\Delta; \epsilon_1, \epsilon_2, \epsilon_3) = 0$ for $\epsilon_2 + \epsilon_3 = 2\Delta$ and $F_3(\Delta; \epsilon_1, \epsilon_2, \epsilon_3) = 0$ for $\epsilon_1 + \epsilon_3 = 2\Delta$, the two-photon related resonances disappear for an undoped system.

Conductivities for Three-Dimensional Massless Dirac Fermions. With the symmetry properties of the conductivities for 2D massive DF in one Dirac cone in hand, and with the

https://dx.doi.org/10.1021/acsphotonics.0c00836
ACS Photonics 2020, 7, 2515−2526

analytic expressions of the conductivities for 2D gapped graphene already determined, we can now turn to the optical response of 3D massless DF. In this work, we focus on the optical response of an isotropic 3D Dirac cone, although more generally, of course, Dirac cones can be anisotropic; this is briefly discussed in "Methods". For 3D massless DFs in a single isotropic Dirac cone, the Hamiltonian[43] is

$$H_{3d}(\boldsymbol{k}) = \hbar v_F \boldsymbol{k}\cdot\boldsymbol{\sigma} \tag{24}$$

where $\boldsymbol{k} = k_x\hat{\boldsymbol{x}} + k_y\hat{\boldsymbol{y}} + k_z\hat{\boldsymbol{z}}$ is a three-dimensional wave vector. The two band energies are $\varepsilon_{\pm k} = \pm\hbar v_F|\boldsymbol{k}|$, which touch at $\boldsymbol{k} = 0$, the Dirac point.

It is the conductivities following from this Hamiltonian in eq 24 that we study here, and we denote them by $\sigma_{3d}^{(1);da}(\omega)$ and $\sigma_{3d}^{(3);dabc}(\omega_1, \omega_2, \omega_3)$. The Hamiltonian $H_{3d}(\boldsymbol{k})$ is spherical symmetric and so the only independent nonzero component of the linear conductivity is $\sigma_{3d}^{(1);xx}(\omega)$; for the third-order conductivity, the independent nonzero components are the symmetric ones $\sigma_{3d}^{(3);xxyy}$, $\sigma_{3d}^{(3);xyxy}$, and $\sigma_{3d}^{(3);xyyx}$. All other components can be obtained either by

$$\sigma_{3d}^{(3);xxxx} = \sigma_{3d}^{(3);xxyy} + \sigma_{3d}^{(3);xyxy} + \sigma_{3d}^{(3);xyyx} \tag{25}$$

or by permutation of the directions $\{x, y, z\}$. Due to the cyclic permutation on $\{a\omega_1, b\omega_2, c\omega_3\}$ of $\sigma_{3d}^{(3);dabc}(\omega_1, \omega_2, \omega_3)$, and all nonzero components can be written in terms of $\sigma_{3d}^{(3);xxyy}(\omega_1, \omega_2, \omega_3)$, which we identify in the following. For a single 3D Dirac cone, the second-order conductivity has nonzero components $\sigma_{3d}^{(2);xyz}(\omega_1, \omega_2) = -\sigma_{3d}^{(2);xzy}(\omega_1, \omega_2)$ and those obtained by permutation of the directions $\{x, y, z\}$. In Dirac semimetals, the total second order responses vanish due to the cancellation between the inversion symmetry related Dirac cones, while they remain in Weyl semimetals without inversion symmetry. However, since any of these nonzero components involves all three directions, the procedure presented below for linear and third-order response functions cannot be applied to second-order response functions.

The Hamiltonian for 3D massless DFs is connected to that of 2D massive DFs through the relation $H_{3d}(\boldsymbol{\kappa} + k_z\hat{\boldsymbol{z}}) = H_{2d}(\boldsymbol{\kappa}, \hbar v_F k_z)$. In the calculation of both the linear and nonlinear conductivities in the independent particle approximation, the full response arises as the sum of the responses of each independent particle, identified initially by its $\boldsymbol{k}$. Thus, the response of 3D massless DFs to electric fields in the x and y directions is equivalent to an ensemble of responses of 2D massive DFs with different gap parameters. In this manner, the linear conductivity can be written as

$$\begin{aligned}\sigma_{3d}^{(1);xx} &= \int \frac{dk_z}{2\pi}\sigma_{2d}^{(1);xx}(\hbar v_F k_z) = \frac{1}{\pi\hbar v_F}\int_0^\infty d\Delta\sigma_{2d}^{(1);xx}(\Delta)\\ &= \frac{1}{4\pi\hbar v_F}\int_0^\infty d\Delta\sigma_{gg}^{(1);xx}(\Delta)\end{aligned} \tag{26}$$

where we have used $\sigma_{2d}^{(1);xx}(\Delta) = \sigma_{2d}^{(1);xx}(-\Delta)$ for the second equal sign and eq 14 for the third equal sign. Similarly, we have

$$\sigma_{3d}^{(3);xxyy} = \frac{1}{4\pi\hbar v_F}\int_0^\infty d\Delta\sigma_{gg}^{(3);xxyy}(\Delta) \tag{27}$$

Once these are determined, all other nonvanishing components of the conductivities for 3D massless DFs follow from the symmetry properties of those tensors.

Using the results for the conductivity of gapped graphene in eqs 16 and 19, the integration can be done analytically, and the result is given in "Methods". Because $\sigma_{gg}^{(1);xx} \propto \Delta^{-1}$ in eq 22, the integration in eq 26 diverges; this is associated with the assumption that the linear dispersion relation continues for all $\boldsymbol{k}$, no matter how large. Taking a cutoff energy E_A as the upper limit of the integration, to model the onset of more realistic band dispersion, the linear conductivity of three-dimensional Dirac Fermions in one cone is

$$\begin{aligned}\sigma_{3d}^{(1);xx}(\omega) &= \sigma_{3d,\mathrm{reg}}^{(1);xx}(\omega) - \frac{ie^2\hbar\omega}{12\pi^2\hbar^2 v_F}\ln\frac{2E_A}{|\mu|},\\ \sigma_{3d,\mathrm{reg}}^{(1);xx}(\omega) &= \frac{ie^2}{24\pi\hbar^2 v_F}\frac{12|\mu|^2 - 5(\hbar\omega)^2 + 3(\hbar\omega)^2\mathcal{Z}(|\mu|;\hbar\omega)}{3\pi\hbar\omega}\end{aligned} \tag{28}$$

where the function $\mathcal{Z}$ is given by

$$\begin{aligned}\mathcal{Z}(|\mu|; w) &= \ln|w^2 - 4\mu^2| - \ln\mu^2\\ &\quad - i\pi\,\mathrm{sgn}(w)\theta(|w| - 2|\mu|)\\ &= \mathcal{T}\left(\frac{w}{|\mu|}\right)\end{aligned} \tag{29}$$

where

$$\mathcal{T}(x) = \ln|x^2 - 4| - i\pi\,\mathrm{sgn}(x)\theta(x - 2) \tag{30}$$

with $\mathrm{sgn}(x)$ the sign function. It is worth noting that E_A is not an cutoff energy for the energies of the DFs, but rather for the gap parameter; hence, the expression in eq 28 is not exactly the same as those in literature that involve an energy cutoff.[45,49,50] However, our result for the real part of the conductivity, which is the physically meaningful term, is consistent with earlier results in literature.

For the third-order conductivity, the integration converges due to $\sigma^{(3);xxyy} \propto \Delta^{-5}$ in eq 23. Therefore, the third-order conductivity of 3D Dirac Fermions is insensitive to the energy cutoff, and it is

$$\begin{aligned}\sigma_{3d}^{(3);xxyy}(\omega_1, \omega_2, \omega_3) &= \frac{iv_F e^4}{16\pi^2}\Bigg\{\frac{8}{45\hbar^3\omega_1\omega_2\omega_3}\\ &+ C_1(\hbar\omega_1, \hbar\omega_2, \hbar\omega_3)\mathcal{Z}(|\mu|; \hbar(\omega_1 + \omega_2 + \omega_3))\\ &+ C_2(\hbar\omega_1, \hbar\omega_2, \hbar\omega_3)\mathcal{Z}(|\mu|; \hbar(\omega_2 + \omega_3))\\ &+ C_3(\hbar\omega_1, \hbar\omega_2, \hbar\omega_3)\mathcal{Z}(|\mu|; \hbar(\omega_1 + \omega_3))\\ &+ C_3(\hbar\omega_1, \hbar\omega_3, \hbar\omega_2)\mathcal{Z}(|\mu|; \hbar(\omega_1 + \omega_2))\\ &+ C_4(\hbar\omega_1, \hbar\omega_2, \hbar\omega_3)\mathcal{Z}(|\mu|; \hbar\omega_1)\\ &+ C_5(\hbar\omega_1, \hbar\omega_2, \hbar\omega_3)\mathcal{Z}(|\mu|; \hbar\omega_2)\\ &+ C_5(\hbar\omega_1, \hbar\omega_3, \hbar\omega_2)\mathcal{Z}(|\mu|; \hbar\omega_3)\}\end{aligned} \tag{31}$$

where C_i is given by

$$\begin{aligned}&C_i(\hbar\omega_l, \hbar\omega_m, \hbar\omega_n)\mathcal{Z}(|\mu|; \hbar\omega)\\ &= \left[\sum_{j=0,2,4}\mathcal{F}_{ij}(\hbar\omega_l, \hbar\omega_m, \hbar\omega_n)\frac{(-\hbar\omega)^{j+1}}{2^{j+1}}\frac{1}{j+1}\right]\mathcal{Z}(|\mu|; \hbar\omega)\end{aligned} \tag{32}$$

Note that the coefficients C_i in $\sigma_{3d}^{(3);xxyy}$ satisfy

$$\begin{aligned}&C_1(\hbar\omega_1, \hbar\omega_2, \hbar\omega_3) + C_2(\hbar\omega_1, \hbar\omega_2, \hbar\omega_3) + C_3(\hbar\omega_1, \hbar\omega_2, \hbar\omega_3)\\ &+ C_3(\hbar\omega_1, \hbar\omega_3, \hbar\omega_2) + C_4(\hbar\omega_1, \hbar\omega_2, \hbar\omega_3) + C_5(\hbar\omega_1, \hbar\omega_2, \hbar\omega_3)\\ &+ C_5(\hbar\omega_1, \hbar\omega_3, \hbar\omega_2) = 0\end{aligned} \tag{33}$$

https://dx.doi.org/10.1021/acsphotonics.0c00836
ACS Photonics 2020, 7, 2515−2526

RESULTS

Since 3D massless DFs form an isotropic system, the current density response can be written as

$$J(t) = \int \frac{d\omega}{2\pi} e^{-i\omega t}\sigma^{(1);xx}(\omega)E_\omega + \int \frac{d\omega_1 d\omega_2 d\omega_3}{(2\pi)^3} e^{-i(\omega_1+\omega_2+\omega_3)t} \times [\sigma_{3d}^{(3);xxyy}(\omega_1, \omega_2, \omega_3)E_{\omega_1}(E_{\omega_2}\cdot E_{\omega_3}) + \sigma_{3d}^{(3);xyxy}(\omega_1, \omega_2, \omega_3) \times E_{\omega_2}(E_{\omega_3}\cdot E_{\omega_1}) + \sigma_{3d}^{(3);xyyx}(\omega_1, \omega_2, \omega_3)E_{\omega_3}(E_{\omega_1}\cdot E_{\omega_2})] \quad (34)$$

where $E_\omega = \int dt E(t)e^{i\omega t}$ is the Fourier transform of the electric field. In this section, we consider the nature of this response for different optical phenomena.

Several General Properties of the Conductivities. We begin by discussing some general properties of the expressions for the linear and third-order conductivities in eqs 28 and 31.

1. For all the nonlinear phenomena we discuss, the third-order conductivity of 3D massless DFs exhibits features very similar to that of graphene,[11,12,24] as we show below, including the appearance of resonances and divergences. In 3D massless DFs, the conductivities involve the function $\mathcal{Z}(|\mu|; \hbar\omega)$, instead of the function $\mathcal{G}(|\mu|; \hbar\omega)$ relevant for graphene. Both functions describe the interband optical transition, but they are weighted by different densities of states. However, there are always singularities at $|\hbar\omega| = 2|\mu|$, around which the real part diverges logarithmically and the imaginary part shows a step function. Similar to the frequency dependence of the nonlinear response of graphene, the third-order conductivity of 3D massless DFs involves photon energies $\hbar\omega_i$, $\hbar\omega_i + \hbar\omega_j$, and $\hbar(\omega_1 + \omega_2 + \omega_3)$, which appear in the second argument of the function $\mathcal{Z}(|\mu|; \hbar\omega)$. Thus, when any of these energies matches $2|\mu|$, a resonant interband transition may appear. When any of these energies is zero, an intraband divergence may appear and lead to a divergent conductivity value in the clean limit at zero temperature.
2. Scaling all energies by the chemical potential, the third-order conductivity can be written as

$$\sigma_{3d}^{(3);dabc}(|\mu|; \omega_1, \omega_2, \omega_3) = \frac{v_F e^4}{16\pi^2|\mu|^3} S_{3d}^{(3);dabc}\left(\frac{\hbar\omega_1}{|\mu|}, \frac{\hbar\omega_2}{|\mu|}, \frac{\hbar\omega_3}{|\mu|}\right) \quad (35)$$

where the dimensionless function $S_{3d}^{(3);dabc}$ can be obtained from $\sigma_{3d}^{(3);dabc}$. To better understand the third-order optical response of 3D massless DFs, we can compare it to that of graphene.[11] If we introduce an effective bulk conductivity of graphene by associating a thickness $d_{\text{eff}} \approx 3.3$ Å with a graphene sheet, that effective bulk third-order conductivity $\sigma_{gh;\text{eff}}^{(3);dabc}$ can be obtained from eq 21 by $\sigma_{\text{gh;eff}}^{(3);dabc} = \sigma_{\text{gh}}^{(3);dabc}/d_{\text{eff}}$, and it can be written as

$$\sigma_{\text{gh;eff}}^{(3);dabc}(|\mu|; \omega_1, \omega_2, \omega_3) = \frac{\hbar v_F^2 e^4}{4\pi d_{\text{eff}}|\mu|^4} S_{\text{gh}}^{(3);dabc}\left(\frac{\hbar\omega_1}{|\mu|}, \frac{\hbar\omega_2}{|\mu|}, \frac{\hbar\omega_3}{|\mu|}\right) \quad (36)$$

where $S_{\text{gh}}^{(3);dabc}$ is a dimensionless function[11] that can be obtained from $\sigma_{\text{gh}}^{(3);dabc}$. Besides the different detailed structures given in the dimensionless functions $S_{3d}^{(3);dabc}$ and $S_{\text{gh}}^{(3);dabc}$, the two conductivities above also show a different dependence on the Fermi velocity v_F and the chemical potential $|\mu|$. Their ratio gives

$$\frac{\sigma_{3d}^{(3);xxyy}}{\sigma_{\text{gh;eff}}^{(3);xxyy}} = \frac{d_{\text{eff}}|\mu|}{4\pi\hbar v_F}\frac{S_{3d}^{(3);xxyy}}{S_{\text{gh}}^{(3);xxyy}} \quad (37)$$

The prefactor is inversely proportional to the Fermi velocity v_F and proportional to the chemical potential $|\mu|$. By taking the Fermi velocity to be that of graphene ($v_F = 10^6$ m/s), the prefactor is about 0.04 for $|\mu| = 1$ eV. Therefore, the third optical conductivity of 3D massless DFs in one Dirac cone is about 2 orders of magnitude smaller than the corresponding effective bulk third order conductivity of graphene. Note that $\sigma_{3d}^{(3);dabc}$ is for one Dirac cone only; if there exists degeneracy g of the Dirac cones, the third order conductivity $\sigma_{3d}^{(3);dabc}$ is g times as large.
3. When all involved frequencies satisfy $\hbar\omega_i/|\mu| \ll 1$, the third-order nonlinear response in a doped Dirac semimetal should be mostly due to the intraband transitions. This limit can be obtained by taking $\hbar\omega_i \to x\hbar\omega_i$ and $x \to 0$, and we find an approximate conductivity is given by

$$\sigma_{3d}^{(3);xxyy}(\omega_1, \omega_2, \omega_3) \approx \frac{iv_F e^4}{16\pi^2}\frac{8}{45\hbar^3\omega_1\omega_2\omega_3} \quad (38)$$

It is independent of the chemical potential $|\mu|$, showing a different dependence on that quantity than that of graphene ($\propto |\mu|^{-1}$). Comparing this conductivity to the effective bulk conductivity of graphene, we find

$$\frac{\sigma_{3d}^{(3);xxyy}}{\sigma_{\text{gh;eff}}^{(3);xxyy}} = \frac{4|\mu|d_{\text{eff}}}{15\pi\hbar v_F} \quad (39)$$

Taking the Fermi velocity to be that of graphene ($v_F = 10^6$ m/s), for $|\mu| = 1$ eV, the ratio is about 0.042.

The expression in eq 38 can be used to evaluate the susceptibility for THG of Cd_3As_2[51] in the terahertz regime directly. Taking a typical frequency $f = 0.8$ THz,[51] with $\omega = 2\pi f$, and an anistropic Fermi velocity[43] $(v_F^x, v_F^y, v_F^z) = (1.28, 1.30, 0.327)v_F$, the susceptibility is obtained from the conductivity (see "Method") as

$$\chi_{3d}^{(3);dddd} = \frac{(v_F^d)^4}{v_F v_F^x v_F^y v_F^z} g_c \frac{3\sigma_{3d}^{(3);xxyy}(\omega, \omega, \omega)}{-i3\omega\epsilon_0} \quad (40)$$

with the cone degeneracy $g_c = 4$. It gives $\chi_{3d}^{(3);xxxx} \approx \chi_{3d}^{(3);yyyy} \approx 2.34 \times 10^{-9}$ m^2/V^2 and $\chi_{3d}^{(3);zzzz} \approx 0.009 \times 10^{-9}$ m^2/V^2. The x and y components are at the same order of magnitude of the experimental value $\sim 10^{-9}$ m^2/V^2.
4. In the undoped limit as the chemical potential $\mu \to 0$, the conductivities depend only on the frequencies. In this limit, the third-order conductivity of graphene is very simple:[11] $\sigma^{(3);xxyy} \propto [(\omega_1 + \omega_2)(\omega_2 + \omega_3)(\omega_3 + \omega_1)(\omega_1 + \omega_2 + \omega_3)]^{-1}$. For 3D massless DFs, the expression for the third-order conductivity in this limit is more complicated. Although the function $\mathcal{Z}(|\mu|; \hbar\omega)$ includes a term $\ln \mu^2$, it does not lead to any divergence because the prefactor vanishes due to eq 33; thus, the conductivity itself has no singularity at $|\mu| = 0$ and is well behaved as $\mu \to 0$.
5. Considering the dependence on the Fermi velocity v_F, the conductivities of graphene give $\sigma_{\text{gh;eff}}^{(n)} \propto v_F^{n-1}$, while those of 3D massless DFs give $\sigma_{3d}^{(n)} \propto v_F^{n-2}$. For graphene, the universal conductance appears in the linear optical

https://dx.doi.org/10.1021/acsphotonics.0c00836
ACS Photonics 2020, 7, 2515−2526

response.[52] For Dirac Fermions, the response independent of the material parameter should occur at second order, and in our simple model, this is absent. But for Weyl semimetals, where inversion symmetry is broken, the universal optical response does appear in the circular photogalvanic effect.[33,37]

Linear Optical Response. For 3D massless DFs, the cutoff energy appears only in the imaginary part of the linear conductivity. The real part in the clean limit is given by

$$\mathrm{Re}[\sigma_{3d}^{(1);xx}(\omega)] = \frac{e^2\omega}{24\pi\hbar v_F}\theta(\hbar\omega - 2|\mu|) \tag{41}$$

which is proportional to the frequency ω. This leads to a frequency independent imaginary part of the susceptibility $\mathrm{Im}[\chi(\omega)] = \mathrm{Re}[\sigma_{3d}^{(1);xx}(\omega)]/(\omega\epsilon_0) = e^2/(24\pi\hbar v_F\epsilon_0)$ for $\hbar\omega > 2|\mu|$, which is inversely proportional to the Fermi velocity v_F. Again, taking the Fermi velocity to be the same as the value for graphene, $v_F = 10^6$ m/s, the absorption coefficient is $\mathrm{Im}[\chi(\omega)] \approx 0.36$.

In the low-frequency regime, the term involving the cutoff energy may contribute little due to its prefactor $\hbar\omega$, and the main contribution comes from the Drude term

$$\sigma_{3d}^{(1);xx}(\omega) \approx \frac{ie^2|\mu|^2}{6\pi^2\hbar^2 v_F}\frac{1}{\hbar\omega} \tag{42}$$

It is proportional to the square of the chemical potential $|\mu|^2$, following the dependence of the density of states. The term $\sigma_{3d,\mathrm{reg}}^{(1);xx}(\omega)$ can be rewritten as

$$\sigma_{3d,\mathrm{reg}}^{(1);xx}(\omega) = \frac{e^2|\mu|}{24\pi\hbar^2 v_F}S_{3d}^{(1)}\left(\frac{\hbar\omega}{|\mu|}\right) \tag{43}$$

with a dimensionless function

$$S_{3d}^{(1)}(x) = \frac{i}{\pi}\frac{12 - 5x^2 + 3x^2\mathcal{T}(x)}{3x} \tag{44}$$

Its real and imaginary parts are plotted in Figure 1. Around $x = 2$, there appears a logarithmic divergence in its imaginary part and a step change in its real part. For $x > 2$, the real part is linearly dependent on x.

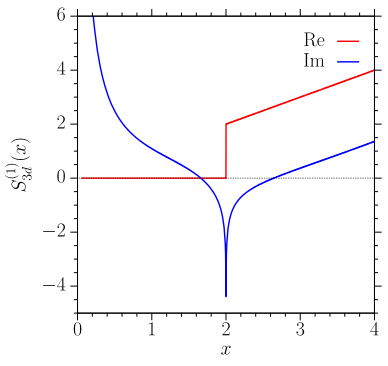

Figure 1. x dependence of $S_{3d}^{(1)}(x)$ for $0 < x < 4$.

Third-Harmonic Generation. The third-order conductivity for THG satisfies $\sigma_{3d}^{(3);xxyy} = \sigma_{3d}^{(3);xyxy} = \sigma_{3d}^{(3);xyyx} = \sigma_{3d}^{(3);xxxx}/3$. The quantity $S_{3d}^{(3);xxyy}(x, x, x)$ is given by

$$S_{3d}^{(3);xxyy}(x, x, x) = \frac{2i}{135x^3}[12 - 5\mathcal{T}(x) + 32\mathcal{T}(2x) - 27\mathcal{T}(3x)] \tag{45}$$

Each $\mathcal{T}$ term is associated with one optical transition involving photon energy $n\hbar\omega$ ($n = 1$, 2, or 3). Similar to the expression for the response tensor describing THG in graphene, the prefactors of these terms have different signs, indicating the existence of interference between these transitions. The real part is

$$\mathrm{Re}[S_{3d}^{(3);xxyy}(x, x, x)] = \frac{2\pi\mathrm{sgn}(x)}{135x^3}[-5\theta(|x| - 2) + 32\theta(2|x| - 2) - 27\theta(3|x| - 2)] \tag{46}$$

For $x > 2$, $\mathrm{Re}[S_{3d}^{(3)}(x, x, x)] = 0$ gives a complete cancellation due to interference. For graphene, the cancellation is not complete.[8,11] In Figure 2, we plot the spectra of $S_{3d}^{(3);xxyy}$ and $S_{\mathrm{gh}}^{(3);xxyy}$. They show very similar amplitudes and structures.

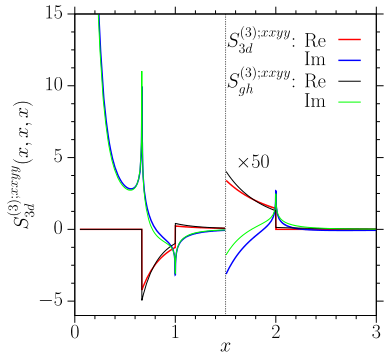

Figure 2. x dependence of $S_{3d}^{(3);xxyy}(x, x, x)$ and $S_{\mathrm{gh}}^{(3);xxyy}(x, x, x)$. Values in the regime $x > 1.5$ are scaled by 50 times.

We close the summary of our results by presenting the conductivity in the limit of $\mu \to 0$. It corresponds to taking $x \to \infty$ in $S_{3d}^{(3);xxyy}(x, x, x)$; thus, the real part is fully canceled and the imaginary part is given by

$$\sigma_{3d}^{(3);xxyy}(\omega, \omega, \omega)|_{\mu=0} = \frac{iv_F e^4(6 + 32\ln 2 - 27\ln 3)}{540\pi^2(\hbar\omega)^3} \tag{47}$$

Finally, we compare our results with those obtained in a velocity gauge using Floquet states by Zhang et al.[43] and Zhong et al.[44] At zero temperature, the real part of their results for one Dirac cone gives

$$\mathrm{Re}[S_{3d}^{(3);xxyy}(x, x, x)]_{\mathrm{lit}} = \frac{2\pi\mathrm{sgn}(x)}{135x^3}[-4\theta(|x| - 2) + 16\theta(2|x| - 2) - 27\theta(3|x| - 2)] \tag{48}$$

with the imaginary part obtained using Kramers–Kronig relations.[43] The results differ from ours in the first two factors for one and two photon resonant processes, and the difference may arise from the choice of the velocity or length gauge to describe the light–matter interaction. Considering the well-known problems that can result using the velocity gauge, a further investigation is required to clarify what causes the different results of these two methods.

Kerr Effect and Two-Photon Absorption. For a monochromatic laser beam, another important optical nonlinearity involves the corrections to the linear response due to the Kerr effect and two-photon absorption, which are described by the tensor $\sigma_{3d}^{(3);dabc}(-\omega, \omega, \omega)$. For the frequency set $(-\omega, \omega, \omega)$, there are only two independent components $\sigma_{3d}^{(3);xxyy}(-\omega, \omega, \omega)$ and $\sigma_{3d}^{(3);xyyx}(-\omega, \omega, \omega) = \sigma_{3d}^{(3);xyxy}(-\omega, \omega, \omega)$. Intraband divergences exist for this third-order conductivity, which are illustrated by

https://dx.doi.org/10.1021/acsphotonics.0c00836
ACS Photonics 2020, 7, 2515–2526

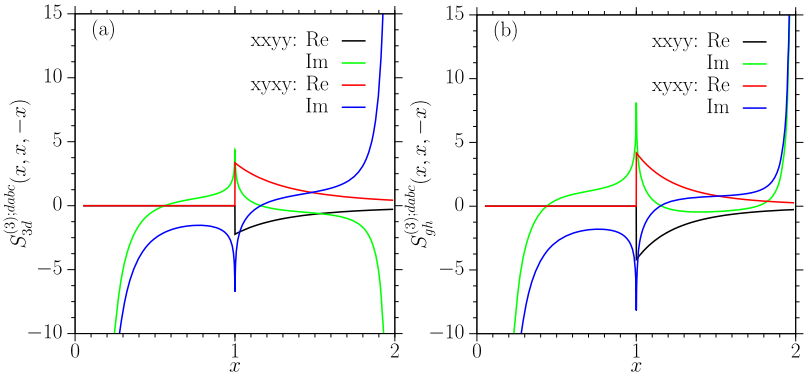

Figure 3. x dependence of (a) $S_{3d}^{(3);dabc}(x, x, -x)$ and (b) $S_{gh}^{(3);dabc}(x, x, -x)$ for the *xxyy* and *xyxy* components.

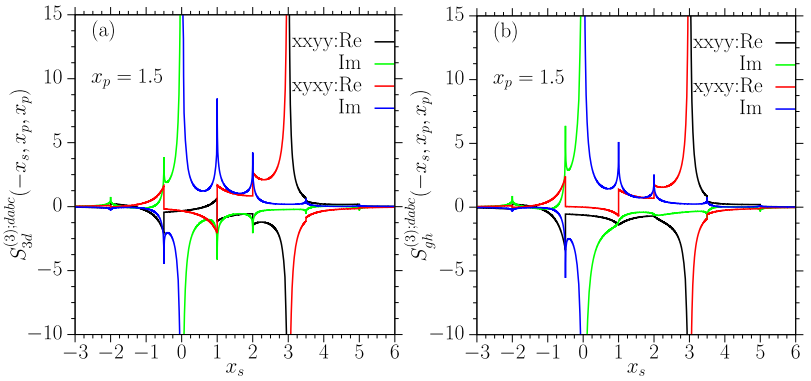

Figure 4. x_s dependence of the spectra for (a) $S_{3d}^{(3);dabc}(-x_s, x_p, x_p)$ for three-dimension massless Dirac Fermions and (b) $S_{gh}^{(3);dabc}(-x_s, x_p, x_p)$ for graphene. The pump frequency is chosen as $x_p = 1.5$.

$$\begin{pmatrix} S_{3d}^{(3);xyxy}(-x,\ x+\delta_1,\ x+\delta_2) \\ S_{3d}^{(3);xxyy}(-x,\ x+\delta_1,\ x+\delta_2) \end{pmatrix} = \frac{4\pi \mathrm{sgn}(x)\theta(x^2-4)}{45w} B_d(x;\delta_1,\delta_2) + B_n(x) + \ldots \tag{49}$$

Here, the first term indicates all the intraband divergences with respect to δ_1 and δ_2, but they are nonzero only when one-photon absorption exists at $|x| > 2$, which is consistent with the general properties of intraband divergences.[24] The function B_d is given by

$$B_d(x;\delta_1,\delta_2) = \frac{\begin{bmatrix}-3\\2\end{bmatrix}}{\delta_1\delta_2} + \frac{\begin{bmatrix}4x+3\delta_2\\-(x+2\delta_2)\end{bmatrix}}{\delta_1(x+\delta_2)(2x+\delta_2)} + \frac{\begin{bmatrix}9x+3\delta_1\\-(x+2\delta_1)\end{bmatrix}}{\delta_2(x+\delta_1)(2x+\delta_1)} \tag{50}$$

The second term B_n is well behaved and given by

$$B_n(x) = \frac{1}{90x^3}\left(\begin{bmatrix}-31\\14\end{bmatrix}\mathcal{T}(-x) + \begin{bmatrix}-65\\50\end{bmatrix}\mathcal{T}(x) + \begin{bmatrix}96\\-64\end{bmatrix}\mathcal{T}(2x) + x\begin{bmatrix}-52\\8\end{bmatrix}\frac{\partial\mathcal{T}(x)}{\partial x} + x^2\begin{bmatrix}-12\\8\end{bmatrix}\frac{\partial^2\mathcal{T}(x)}{\partial x^2} - 16\begin{bmatrix}1\\1\end{bmatrix}\right) \tag{51}$$

In Figure 3 we plot $S_{3d}^{(3);dabc}(-x, x, x)$ for $0 < x < 2$ and compare it with $S_{gh}^{(3);dabc}(-x, x, x)$. In general, both functions show very similar structures and amplitudes, except for two obvious differences: (1) $\mathrm{Im}[S_{3d}^{(3);xxyy}]$ diverges to $-\infty$ as $x \to 2$, while $\mathrm{Im}[S_{gh}^{(3);xxyy}]$ diverges to $+\infty$; (2) For graphene, the real parts of these two components satisfy $\mathrm{Re}[S_{gh}^{(3);xxyy}] = -\mathrm{Re}[S_{gh}^{(3);xyxy}]$; however, for 3D massless DFs $S_{3d}^{(3);xxyy}$ this does not hold. For $x > 2$, the intraband divergences dominate, and in practice both the relaxation processes and pulse shape effects will determine the magnitude of the response. As a comparison, in the clean limit the results of Zhong et al.,[44] Zhang et al.,[43] and Ooi et al.[42,45] give $\mathrm{Re}[\sigma_{3d}^{(3);xxxx}] \propto \theta(\hbar\omega - 2|\mu|)$, which contains no two-photon absorption. (The results in ref 44 have an obvious typographical error, as a comparison with those in ref 43.) We are not sure whether or not such a difference occurs due to the different choices for the light–matter interaction.

Next we present our results for two-photon carrier injection. When one-photon absorption is absent ($x < 2$), the two-photon absorption coefficient can be calculated through $\xi_2^{abcd}(\omega) = 3(\hbar\omega)^{-1}\mathrm{Re}[\sigma^{(3);abcd}(-\omega, \omega, \omega)]$.[11] It can be written as

$$\begin{pmatrix} \xi_2^{xyxy}(\omega) \\ \xi_2^{xxyy}(\omega) \end{pmatrix} = \frac{v_F e^4}{240\pi|\mu|^4}\ \mathrm{sgn}(\omega) X\left(\frac{\hbar\omega}{|\mu|}; \frac{\hbar\delta_1}{|\mu|}, \frac{\hbar\delta_2}{|\mu|}\right) \tag{52}$$

with

$$X(x;\delta_1,\delta_2) = -\frac{4}{x^2}B_d(x;\delta_1,\delta_2)\theta(x^2-4) + \frac{1}{x^4}\begin{pmatrix} 48\theta(x^2-1) - 17\theta(x^2-4) \\ -32\theta(x^2-1) + 18\theta(x^2-4) \end{pmatrix} \tag{53}$$

The first term comes from the intraband divergences, part of which enters in the second term giving contributions proportional to $\theta(x^2 - 4)$. The first term exists only in the presence of one-photon absorption ($x > 2$), and physically, the divergences are induced by the stimulated Raman scattering process. For $1 < x < 2$ (i.e., $|\mu| < \hbar\omega < 2|\mu|$), two-photon absorption gives

https://dx.doi.org/10.1021/acsphotonics.0c00836
ACS Photonics 2020, 7, 2515−2526

$$\begin{pmatrix}\xi_2^{xyxy}(\omega)\\ \xi_2^{xxyy}(\omega)\end{pmatrix} = \frac{v_F e^4}{15\pi(\hbar\omega)^4}\begin{pmatrix}3\\-2\end{pmatrix} \tag{54}$$

Compared to the results for graphene, the frequency dependence changes from ω^{-5} to ω^{-4}.

Parametric Frequency Conversion. When there are two laser beams, one with pump frequency ω_p and the second with signal frequency ω_s, a new frequency $2\omega_p - \omega_s$ can be generated through parametric frequency conversion (PFC); the current density responsible for it is determined by $\sigma_{3d}^{(3);dabc}(-\omega_s, \omega_p, \omega_p)$. For 3D massless DFs, this process has only two independent components: $\sigma_{3d}^{(3);xxyy}$ and $\sigma_{3d}^{(3);xyxy} = \sigma_{3d}^{(3);xyyx}$. Defining $x_{s,p} \equiv \hbar\omega_{s,p}/|\mu|$, the term $S_{3d}^{(3);dabc}(-x_s, x_p, x_p)$ shows interband divergences under the conditions $x_s = \pm 2$, $x_p = \pm 2$, $x_p = \pm 1$, $x_p - x_s = \pm 2$, or $2x_p - x_s = \pm 2$, and intraband divergences at $2x_p - x_s = 0$, $x_s = 0$. As an illustration, we fix $x_p = 1.5$ and show different components in Figure 4. The possible divergences appear at $x_s = -2, -0.5, 1, 3$, and 3.5 (interband), and at $x_s = 0$ and 5 (intraband). All these divergences exist for $S_{3d}^{(3);dabc}$, but two of these divergences, those at $x_s = 1$ and 2, are removed for $S_{gh}^{(3);dabc}$. Both conductivities exhibit similar amplitudes and structures. For the intraband divergences, that at $x_s = 0$ is associated with a field/current-induced second-harmonic generation, and the other at $x_s = 2x_p$ corresponds to two-color CCI, which is discussed in the next section. Around these two divergences, the conductivities diverge as x_s^{-1} around $x_s \sim 0$, and $(x_s - 2x_p)^{-1}$ as $x_s \sim 2x_p$. Obviously, the spectra diverge much faster around intraband divergences than around interband divergences, where the divergences are logarithmic.

Two-Color Coherent Current Injection. The intraband divergence of $\sigma_{3d}^{(3);dabc}(-\omega, -\omega, 2\omega + \delta)$ as $\delta \to 0$ corresponds to a well-known nonlinear phenomenon, two-color coherent current injection, in which a quasi-static current can be generated due to the interference of one-photon absorption and two-photon absorption processes. The divergence means that the current is continually injected or

$$\frac{dJ^a(t)}{dt} = \eta_{3d}^{abcd}(\omega)E_{-\omega}^b E_{-\omega}^c E_{2\omega}^d + c.c. \tag{55}$$

with

$$\eta_{3d}^{abcd}(\omega) = \lim_{\delta\to 0}[-3i\delta\sigma_{3d}^{(3);abcd}(-\omega, -\omega, 2\omega + \delta)] \tag{56}$$

After simple algebra, for $\omega > 0$, we get

$$\begin{pmatrix}\eta_{3d}^{xxyy}(\omega)\\ \eta_{3d}^{xyyx}(\omega)\end{pmatrix} = \frac{iv_F e^4}{60\pi(\hbar\omega)^2}\left[\begin{pmatrix}-6\\4\end{pmatrix}\theta(\hbar\omega - |\mu|) + \begin{pmatrix}2\\-3\end{pmatrix}\theta(\hbar\omega - 2|\mu|)\right] \tag{57}$$

The term involving $\theta(\hbar\omega - |\mu|)$ is associated with the interference between the transition channels induced by a two-photon absorption $(\omega + \omega)$ and a one-photon absorption (2ω), while the other term involving $\theta(\hbar\omega - 2|\mu|)$ is associated with the interference of stimulated electronic Raman scattering (for photon frequencies 2ω and $-\omega$) and one-photon absorption (ω). Compared to the injection in graphene, the injection coefficients in 3D massless DFs are proportional to $(\hbar\omega)^{-2}$, instead of $(\hbar\omega)^{-3}$ in graphene;[11] the relative amplitudes between different components are also different.

CONCLUSION AND DISCUSSION

We have calculated the linear and third order conductivities for a single Dirac cone of 3D massless Dirac Fermions. In our simple model, we treat the light−matter interaction in the length gauge, in which the kind of unphysical divergences associated with band truncation that can appear in the velocity gauge do not arise. Analytic expressions for general input frequencies were obtained in the clean limit at zero temperature. Utilizing these expressions, we discussed in detail the frequency dependence of THG, the Kerr effect and two-photon absorption, parametric frequency conversion, and two-color coherent current injection. The dimension affects the optical response of Dirac Fermions in several ways, and a comparison between two and three-dimensional massless Dirac Fermions allows us to identify the following qualitative features: (1) the dependence on the Fermi velocity v_F, which is the relevant material parameter in these systems, changes from v_F^{n-1} in 2D to v_F^{n-2} in 3D for the nth order conductivity, (2) the chemical potential dependence of the third order conductivity changes from μ^{-1} to μ^0 for a lightly doped sample, (3) the frequency dependence of the two photon carrier injection changes from ω^{-5} to ω^{-4}, (4) the frequency dependence of two color current injection changes from ω^{-3} to ω^{-2}, and (5) for nonzero chemical potential, both frequency spectra show very similar structures in general, but their amplitude can differ up to 2 orders of magnitude. We emphasize that despite of the smaller nonlinear conductivities, strong and tunable nonlinear response could be generated from materials hosting 3D Dirac Fermions by changing the sample thickness, a tuning parameter not available for 2D materials.

Although our results are obtained in the clean limit at zero temperature, they provide a general picture for third order response in three-dimensional massless Dirac Fermions, and they can be treated as a starting point for future study in nonlinear response of Dirac and Weyl semimetals.

Finally, we discuss the inclusion of phenomenological relaxation parameters and finite temperature, both of which are straightforward. For the third order conductivity of gapped graphene in our previous work,[24] the gap parameter appears in the conductivities as functions of $1/E_c^i$ $(i = 1, 3, 5)$, $\Delta^n\mathcal{G}(E_c; w)$, $\Delta^n\mathcal{H}(E_c; w) = \frac{\partial}{\partial w}[\Delta^n\mathcal{G}(E_c; w)]$, and $\Delta^n\mathcal{I}(E_c; w) = -\frac{\partial}{\partial w}[\Delta^n\mathcal{H}(E_c; w)]$ for $n = 0$, 2, and 4. The integration of the latter two functions with respect to Δ can be derived from those for $\Delta^n\mathcal{G}(E_c; w)$. The integrations of $\int_0^{E_A} E_c^{-i} d\Delta$ can also be obtained easily. Therefore, the third-order conductivity with finite phenomenological relaxation parameters can be obtained by replacing $\Delta^n\mathcal{G}(E_c; w) \to \mathcal{Y}_n(|\mu|; w)$, $\Delta^n\mathcal{H}(E_c; w) \to \frac{\partial}{\partial w}\mathcal{Y}_n(|\mu|; w)$, and $\Delta^n\mathcal{I}(E_c; w) \to -\frac{\partial^2}{\partial w^2}\mathcal{Y}_n(|\mu|; w)$, and leaving the divergent terms with respect to E_A in the integration of $\int_0^{E_A} E_c^{-i} d\Delta$. The complicated but analytic expressions could be evaluated numerically. Starting from the chemical potential dependence of the conductivity $\sigma_{3d}^{(1);xx}(|\mu|;\omega)$ and $\sigma_{3d}^{(3);xxyy}(|\mu|;\omega_1, \omega_2, \omega_3)$ at zero temperature, the corresponding dependence at finite temperature can be constructed using the technique presented earlier.[12] With this in hand, an investigation of the effects of the relaxation parameter and finite temperature on the optical conductivities of three-dimensional Dirac Fermions can be undertaken.

https://dx.doi.org/10.1021/acsphotonics.0c00836
ACS Photonics 2020, 7, 2515−2526

However, we want to emphasize that even with such a treatment of phenomenological relaxation parameters and the consideration of finite temperature, a detailed comparison with experiments on materials exhibiting three-dimensional massless Dirac Fermions only makes sense for low-light frequencies due to a small energy range over which the assumption of a linear regime in the band dispersion is valid. While experiments on the Dirac semimetal Cd_3As_2 indicate that the energy scale of the linear regime could be as large as about an electronvolt, most theoretical calculations of Dirac semimetals limit this linear regime to a few tens of millielectron volts.[53] Realistic calculations based on full band structures will be required. Nonetheless, the study we have presented here will serve as a benchmark for identifying when those full band structure calculations show a significant difference from ideal Dirac Fermion behavior.

METHODS

Comparing Responses. We consider the relation between the optical conductivities of two different systems with Hamiltonians, $H^A(\boldsymbol{k})$ and $H^B(\boldsymbol{k})$, that are connected via a unitary matrix U and a real matrix R through

$$UH^A((R^T)^{-1}\boldsymbol{k})U^\dagger = H^B(\boldsymbol{k}) \tag{58}$$

The dynamics of these two systems can be described by density matrices $\rho^A_{\boldsymbol{k}}(t)$ and $\rho^B_{\boldsymbol{k}}(t)$. Under the application of electric field $\boldsymbol{E}(t)$, they satisfy the equation of motion[11]

$$\hbar\partial_t\rho^A_{\boldsymbol{k}}(t) = -i[H^A(\boldsymbol{k}), \rho^A_{\boldsymbol{k}}(t)] + e\boldsymbol{E}(t)\cdot\nabla_{\boldsymbol{k}}\rho^A_{\boldsymbol{k}}(t) \tag{59}$$

$$\hbar\partial_t\rho^B_{\boldsymbol{k}}(t) = -i[H^B(\boldsymbol{k}), \rho^B_{\boldsymbol{k}}(t)] + e\boldsymbol{E}(t)\cdot\nabla_{\boldsymbol{k}}\rho^B_{\boldsymbol{k}}(t) \tag{60}$$

To clearly indicate the field that leads to the response, we denote the solutions of these two equations as $\rho^{A/B}_{\boldsymbol{k}}(t; \boldsymbol{E}(t))$. The current density responses are functionals of the field $\boldsymbol{E}(t)$ and can be calculated as

$$\boldsymbol{J}^A(t; \boldsymbol{E}(t)) = -\frac{e}{\hbar}\sum_{\boldsymbol{k}} \mathrm{Tr}[\rho^A_{\boldsymbol{k}}(t; \boldsymbol{E}(t))\nabla_{\boldsymbol{k}}H^A(\boldsymbol{k})] \tag{61}$$

$$\boldsymbol{J}^B(t; \boldsymbol{E}(t)) = -\frac{e}{\hbar}\sum_{\boldsymbol{k}} \mathrm{Tr}[\rho^B_{\boldsymbol{k}}(t; \boldsymbol{E}(t))\nabla_{\boldsymbol{k}}H^B(\boldsymbol{k})] \tag{62}$$

Now we determine the connection between $\rho^A_{\boldsymbol{k}}(t; \boldsymbol{E}(t))$ and $\rho^B_{\boldsymbol{k}}(t; \boldsymbol{E}(t))$ induced by the relation in eq 58. Considering a transformation

$$\bar{\rho}_{\boldsymbol{k}}(t) = U\rho^A_{(R^T)^{-1}\boldsymbol{k}}(t; \boldsymbol{E}(t))U^{-1} \tag{63}$$

from eq 59, the dynamics of $\bar{\rho}_{\boldsymbol{k}}(t)$ is

$$\hbar\partial_t\bar{\rho}_{\boldsymbol{k}}(t) = -i[UH^A((R^T)^{-1}\boldsymbol{k})U^{-1}, \bar{\rho}_{\boldsymbol{k}}(t)] + e[R^T\boldsymbol{E}(t)]\cdot\nabla_{\boldsymbol{k}}\bar{\rho}_{\boldsymbol{k}}(t) \tag{64}$$

Utilizing eq 58, it is transformed into eq 60, and we can find the solution is

$$\bar{\rho}_{\boldsymbol{k}}(t) = \rho^B_{\boldsymbol{k}}(t; R^T\boldsymbol{E}(t)) \tag{65}$$

Then from eq 63 the connection between $\rho^A_{\boldsymbol{k}}(t)$ and $\rho^B_{\boldsymbol{k}}(t)$ is

$$\rho^B_{\boldsymbol{k}}(t; R^T\boldsymbol{E}(t)) = U\rho^A_{(R^T)^{-1}\boldsymbol{k}}(t; \boldsymbol{E}(t))U^{-1} \tag{66}$$

In eq 62, by replacing $\boldsymbol{E}(t) \to R^T\boldsymbol{E}(t)$ and utilizing eq 66 and then comparing to eq 61, we get

$$\boldsymbol{J}^A(t; \boldsymbol{E}(t)) = |R^{-1}|R\boldsymbol{J}^B(t; R^T\boldsymbol{E}(t)) \tag{67}$$

For a weak electric field $\boldsymbol{E}(t)$, the induced current density can be expanded in a power series of this field, and the expansion coefficients are the conductivity tensors, which satisfy

$$\sigma^{(1);da}_A = |R^{-1}|R^{dd'}R^{aa'}\sigma^{(1);d'a'}_B \tag{68}$$

$$\sigma^{(3);dabc}_A = |R^{-1}|R^{dd'}R^{aa'}R^{bb'}R^{cc'}\sigma^{(3);d'a'b'c'}_B \tag{69}$$

Note that for all of these analyses, R is not limited to be a orthogonal matrix, and therefore such transformation can be used to connect the response of an anisotropic Dirac cone, that is, $H^A(\boldsymbol{k}) = \hbar v_F\boldsymbol{k}\cdot R\cdot\boldsymbol{\sigma}$, to that of an isotropic cone $H^B(\boldsymbol{k}) = \hbar v_F\boldsymbol{k}\cdot\boldsymbol{\sigma}$. For an anisotropic Dirac cone with Fermi velocities v^d_F along the d direction, the R matrix has only diagonal components $R^{dd} = v^d_F/v_F$, then the conductivity for an anisotrpic Dirac cone σ_A can be obtained from those for an isotropic one σ_B as

$$\sigma^{(1);da}_A = \frac{v_F v^d_F v^a_F}{v^x_F v^y_F v^z_F}\sigma^{(1);da}_B \tag{70}$$

$$\sigma^{(3);dabc}_A = \frac{v^d_F v^a_F v^b_F v^c_F}{v_F v^x_F v^y_F v^z_F}\sigma^{(3);dabc}_B \tag{71}$$

Expressions of $\mathcal{F}_{ij}$ for Gapped Graphene. Using $\epsilon_{ij} = \epsilon_i + \epsilon_j$ and $\epsilon = \epsilon_1 + \epsilon_2 + \epsilon_3$, we write

$$\mathcal{F}_{ij}(\epsilon_1, \epsilon_2, \epsilon_3) = \frac{\bar{\mathcal{F}}_{ij}(\epsilon_1, \epsilon_2, \epsilon_3)}{6\epsilon_1^2\epsilon_2^2\epsilon_3^2\epsilon_{12}\epsilon_{23}\epsilon_{31}\epsilon} \tag{72}$$

where $\bar{\mathcal{F}}_{ij}(\epsilon_1, \epsilon_2, \epsilon_3)$ are given by

$$\bar{\mathcal{F}}_{10}(\epsilon_1, \epsilon_2, \epsilon_3) = \epsilon^2[3\epsilon_1^3\epsilon_{23} + (-\epsilon_2\epsilon_3 + 2\epsilon_1^2 - \epsilon_1\epsilon_{23})\epsilon_{23}^2 + \epsilon_1\epsilon_2\epsilon_3(2\epsilon_{23} - \epsilon_1)] \tag{73}$$

$$\bar{\mathcal{F}}_{12}(\epsilon_1, \epsilon_2, \epsilon_3) = -8[3\epsilon_1^2\epsilon_2\epsilon_3 + \epsilon_1^3\epsilon_{23} - \epsilon_{23}^2(\epsilon_2\epsilon_3 + \epsilon_1\epsilon_{23})] \tag{74}$$

$$\bar{\mathcal{F}}_{14}(\epsilon_1, \epsilon_2, \epsilon_3) = -16(\epsilon_2\epsilon_3 + \epsilon_1\epsilon_{23}) \tag{75}$$

$$\bar{\mathcal{F}}_{20}(\epsilon_1, \epsilon_2, \epsilon_3) = \epsilon_{12}\epsilon_{13}\epsilon_{23}^4 \tag{76}$$

$$\bar{\mathcal{F}}_{22}(\epsilon_1, \epsilon_2, \epsilon_3) = -8\epsilon_{12}\epsilon_{13}\epsilon_{23}^2 \tag{77}$$

$$\bar{\mathcal{F}}_{24}(\epsilon_1, \epsilon_2, \epsilon_3) = 16\epsilon_{12}\epsilon_{13} \tag{78}$$

$$\bar{\mathcal{F}}_{30}(\epsilon_1, \epsilon_2, \epsilon_3) = -\epsilon_{12}\epsilon_{13}^2\epsilon_{23}[3\epsilon_1^2 + 2\epsilon_1\epsilon_2 - 3\epsilon_2\epsilon_3 + (2\epsilon_1 - \epsilon_3)\epsilon_{23}] \tag{79}$$

$$\bar{\mathcal{F}}_{32}(\epsilon_1, \epsilon_2, \epsilon_3) = 8\epsilon_{12}(\epsilon_1 - \epsilon_3)\epsilon_{23}(\epsilon + \epsilon_2) \tag{80}$$

$$\bar{\mathcal{F}}_{34}(\epsilon_1, \epsilon_2, \epsilon_3) = 16\epsilon_{12}\epsilon_{23} \tag{81}$$

$$\bar{\mathcal{F}}_{40}(\epsilon_1, \epsilon_2, \epsilon_3) = \epsilon_1^2[\epsilon_2\epsilon_3(\epsilon + \epsilon_{23})^2 + \epsilon(\epsilon - \epsilon_{23})\epsilon_{23}(3\epsilon + \epsilon_{23})] \tag{82}$$

$$\bar{\mathcal{F}}_{42}(\epsilon_1, \epsilon_2, \epsilon_3) = -8[\epsilon^3\epsilon_{23} - \epsilon\epsilon_{23}^3 + \epsilon_2\epsilon_3(-3\epsilon^2 + \epsilon_{23}^2)] \tag{83}$$

$$\bar{\mathcal{F}}_{44}(\epsilon_1, \epsilon_2, \epsilon_3) = -16(-\epsilon_2\epsilon_3 + \epsilon_{23}\epsilon) \tag{84}$$

$$\bar{\mathcal{F}}_{50}(\epsilon_1, \epsilon_2, \epsilon_3) = -\epsilon_2^2[\epsilon\epsilon_1(\epsilon_{23} + \epsilon_3)^2 + \epsilon_2\epsilon_3\epsilon_{23}(\epsilon_{23} + 3\epsilon_3)] \tag{85}$$

$$\bar{\mathcal{F}}_{52}(\epsilon_1, \epsilon_2, \epsilon_3) = 8(-\epsilon_3^3\epsilon_{23} + \epsilon_3\epsilon_{23}^3 - 3\epsilon_1\epsilon_3^2\epsilon + \epsilon_1\epsilon_{23}^2\epsilon) \tag{86}$$

$$\bar{\mathcal{F}}_{54}(\epsilon_1, \epsilon_2, \epsilon_3) = -16(\epsilon_3\epsilon_{23} + \epsilon_1\epsilon) \tag{87}$$

Conductivity for 3D Dirac Fermions. The linear conductivity and third order conductivity of three-dimensional

https://dx.doi.org/10.1021/acsphotonics.0c00836
ACS Photonics 2020, 7, 2515−2526

Dirac Fermions are constructed from eqs 26 and 27, respectively. The upper limit of the integration is infinity, and thus it is necessary to introduce a cutoff energy A to analyze the integration

$$I^{(n)}(A) = \frac{1}{4\pi\hbar v_F}\int_0^A d\Delta\sigma_{gg}^{(n)}(\Delta) \tag{88}$$

and then $\sigma_{3d}^{(n)} = \lim_{A\to\infty} I^{(n)}(A)$. As $\Delta \to \infty$, from eqs 22 and 23, we have $\sigma_{gg}^{(1);xx}(\Delta \to \infty) \to -4i\sigma_0\hbar\omega/(3\pi)\Delta^{-1}$ and $\sigma_{gg}^{(3);xxyy}(\Delta \to \infty) \sim \Delta^{-5}$. It is obvious that $I^{(1);xx}(A \to \infty)$ diverges as $\ln A$ and $I^{(3);xxyy}(A \to \infty)$ converges.

The Δ dependence in the conductivities of gapped graphene appears in Δ or $\Delta^n\mathcal{G}(E_c; w)$ for $n = 0$, 2, and 4. By extending the definition of $\mathcal{G}(E_c; w)$ to a complex $w = w_r + iw_i$, we get

$$\mathcal{G}(E_c; w) = i\pi + \mathcal{L}(E_c; w) - \mathcal{L}(-E_c; w) \tag{89}$$

with

$$\mathcal{L}(x; w_r + iw_i) = \frac{1}{2}\ln[(w_r + 2x)^2 + w_i^2] - i\arctan\frac{w_r + 2x}{w_i} \tag{90}$$

As $w_i \to 0^+$, it becomes

$$\mathcal{L}(x; w_r) = \ln|w_r + 2x| - i\frac{\pi}{2}\,\mathrm{sgn}(w_r + 2x) \tag{91}$$

with $\mathrm{sgn}(x)$ as the sign function.

For the term $\Delta^n\mathcal{G}(E_c; w)$, the integration is

$$\begin{aligned}&\int_0^{E_A} x^n\mathcal{G}(\max\{|\mu|, x\}; w)\mathrm{d}x\\ &= \int_0^{|\mu|} x^n\mathcal{G}(|\mu|; w)\mathrm{d}x + \int_{|\mu|}^{E_A} x^n\mathcal{G}(x; w)\mathrm{d}x\\ &= \frac{|\mu|^{n+1}}{n+1}\mathcal{G}(|\mu|; w) + \mathcal{K}_n(E_A; w) - \mathcal{K}_n(|\mu|; w)\end{aligned} \tag{92}$$

with

$$\mathcal{K}_n(x; w) = \frac{1}{n+1}[x^{n+1}\mathcal{G}(x; w) - \mathcal{Q}_n(x; w)] \tag{93}$$

$$\begin{aligned}\mathcal{Q}_n(x; w) = &\frac{(-w)^{n+1}}{2^{n+1}}[\mathcal{L}(x; w) + (-1)^n\mathcal{L}(-x; w)]\\ &+ \frac{1}{2^{n+1}}\sum_{m=1}^{n+1} C_{n+1}^m\frac{(-w)^{n+1-m}}{m}[(w + 2x)^m\\ &- (-1)^{n+1}(w - 2x)^m]\end{aligned} \tag{94}$$

Taking $A \to \infty$, $\mathcal{K}_n(A; w)$ diverges as $\propto\ln(2E_A)$, E_A^2, and E_A^4 for $n = 0$, 2, and 4. We collect all divergent terms into $\mathcal{R}_n(A; w)$ and write $\mathcal{K}_n(E_A; w) = \bar{\mathcal{K}}_n(w) + \mathcal{R}_n(E_A; w)$ with

$$\bar{\mathcal{K}}_0(w) = 0,\ \bar{\mathcal{K}}_2(w) = -\frac{1}{8}w^3,\ \bar{\mathcal{K}}_4(w) = -\frac{5}{192}w^5 \tag{95}$$

Therefore, the integration becomes

$$\int_0^{E_A} x^n\mathcal{G}(\max\{|\mu|, x\}; w)\mathrm{d}x = \mathcal{Y}_n(|\mu|; w) + \mathcal{R}_n(A; w) \tag{96}$$

with

$$\mathcal{Y}_n(|\mu|; w) = \bar{\mathcal{K}}_n(w) + \frac{1}{n+1}\mathcal{Q}_n(|\mu|; w) \tag{97}$$

Now we can construct the conductivity $\sigma_{3d}^{(n)}$ from that of $\sigma_{gg}^{(n)}$ by replacing $\Delta^n\mathcal{G}(E_c; w)$ with $\mathcal{Y}_n(|\mu|; w)$. For the linear conductivity $\sigma_{3d}^{(1);xx}(\omega)$, the divergent term can be obtained from eq 22 directly. Based on eq 19, in the clean limit the third order conductivity for Dirac Fermions is

$$\begin{aligned}&\sigma_{3d}^{(3);xxyy}(|\mu|; \omega_1, \omega_2, \omega_3)\\ &= \frac{iv_Fe^4}{16\pi^2}\sum_{j=0,2,4}\{\mathcal{F}_{1j}(\hbar\omega_1, \hbar\omega_2, \hbar\omega_3)\mathcal{Y}_j(|\mu|; \hbar(\omega_1 + \omega_2 + \omega_3))\\ &+ \mathcal{F}_{2j}(\hbar\omega_1, \hbar\omega_2, \hbar\omega_3)\mathcal{Y}_j(|\mu|; \hbar(\omega_2 + \omega_3))\\ &+ \mathcal{F}_{3j}(\hbar\omega_1, \hbar\omega_2, \hbar\omega_3)\mathcal{Y}_j(|\mu|; \hbar(\omega_1 + \omega_3))\\ &+ \mathcal{F}_{3j}(\hbar\omega_1, \hbar\omega_3, \hbar\omega_2)\mathcal{Y}_j(|\mu|; \hbar(\omega_1 + \omega_2))\\ &+ \mathcal{F}_{4j}(\hbar\omega_1, \hbar\omega_2, \hbar\omega_3)\mathcal{Y}_j(|\mu|; \hbar\omega_1)\\ &+ \mathcal{F}_{5j}(\hbar\omega_1, \hbar\omega_2, \hbar\omega_3)\mathcal{Y}_j \times (|\mu|; \hbar\omega_2)\\ &+ \mathcal{F}_{5j}(\hbar\omega_1, \hbar\omega_3, \hbar\omega_2)\mathcal{Y}_j(|\mu|; \hbar\omega_3)\}\end{aligned} \tag{98}$$

It can be simplified in terms of the function $\mathcal{L}(x; w) + \mathcal{L}(-x; w)$, and we then get the expression in eq 31.

AUTHOR INFORMATION

Corresponding Author

J. L. Cheng − *State Key Laboratory of Applied Optics, Changchun Institute of Optics, Fine Mechanics and Physics, Chinese Academy of Sciences, Changchun 130033, China; School of Physical Sciences, University of Chinese Academy of Sciences, Beijing 100049, China;* orcid.org/0000-0003-4875-9342; Email: jlcheng@ciomp.ac.cn

Authors

J. E. Sipe − *Department of Physics, University of Toronto, Toronto, Ontario, Canada*

S. W. Wu − *State Key Laboratory of Surface Physics, Key Laboratory of Micro and Nano Photonic Structures (MOE), and Department of Physics, Fudan University, Shanghai 200433, China;* orcid.org/0000-0001-9838-9066

Complete contact information is available at: https://pubs.acs.org/10.1021/acsphotonics.0c00836

Notes

The authors declare no competing financial interest.

ACKNOWLEDGMENTS

This work has been supported by K. C. Wong Education Foundation Grant No. GJTD-2018-08, Scientific Research Project of the Chinese Academy of Sciences Grant No. QYZDB-SSW-SYS038, and National Natural Science Foundation of China Grant Nos. 11774340 and 61705227. S.W.W. is supported by the National Key Research and Development Program of China (Grant No. 2019YFA0308404). J.E.S. is supported by the Natural Sciences and Engineering Research Council of Canada. J.L.C. acknowledges the support from "Xu Guang" Talent Program of CIOMP.

REFERENCES

(1) Castro Neto, A. H.; Guinea, F.; Peres, N. M. R.; Novoselov, K. S.; Geim, A. K. The electronic properties of graphene. *Rev. Mod. Phys.* **2009**, *81*, 109−162.

(2) Ferrari, A. C.; et al. Science and technology roadmap for graphene, related two-dimensional crystals, and hybrid systems. *Nanoscale* **2015**, *7*, 4598−4810.

(3) Bonaccorso, F.; Sun, Z.; Hasan, T.; Ferrari, A. C. Graphene photonics and optoelectronics. *Nat. Photonics* **2010**, *4*, 611−622.

(4) Glazov, M.; Ganichev, S. High frequency electric field induced nonlinear effects in graphene. *Phys. Rep.* **2014**, *535*, 101−138.

(5) Ooi, K. J. A.; Tan, D. T. H. Nonlinear graphene plasmonics. *Proc. R. Soc. London, Ser. A* **2017**, *473*, 20170433.

(6) Gu, T.; Petrone, N.; McMillan, J. F.; van der Zande, A.; Yu, M.; Lo, G. Q.; Kwong, D. L.; Hone, J.; Wong, C. W. Regenerative oscillation and four-wave mixing in graphene optoelectronics. *Nat. Photonics* **2012**, *6*, 554−559.
(7) Vermeulen, N.; Castello-Lurbe, D.; Khoder, M.; Pasternak, I.; Krajewska, A.; Ciuk, T.; Strupinski, W.; Cheng, J.; Thienpont, H.; Van Erps, J. Graphene's nonlinear-optical physics revealed through exponentially growing self-phase modulation. *Nat. Commun.* **2018**, *9*, 2675.
(8) Jiang, T.; et al. Gate-tunable third-order nonlinear optical response of massless Dirac fermions in graphene. *Nat. Photonics* **2018**, *12*, 430−436.
(9) Soavi, G.; et al. Broadband, electrically tunable third-harmonic generation in graphene. *Nat. Nanotechnol.* **2018**, *13*, 583−588.
(10) Mikhailov, S. A. Non-linear electromagnetic response of graphene. *Europhys. Lett.* **2007**, *79*, 27002.
(11) (a) Cheng, J. L.; Vermeulen, N.; Sipe, J. E. Third order optical nonlinearity of graphene. *New J. Phys.* **2014**, *16*, 053014. (b) Cheng, J. L.; Vermeulen, N.; Sipe, J. E. Corrigendum: Third order optical nonlinearity of graphene (2014 New J. Phys. 16 053014). *New J. Phys.* **2016**, *18*, 029501.
(12) (a) Cheng, J. L.; Vermeulen, N.; Sipe, J. E. Third-order nonlinearity of graphene: Effects of phenomenological relaxation and finite temperature. *Phys. Rev. B: Condens. Matter Mater. Phys.* **2015**, *91*, 235320. (b) Cheng, J. L.; Vermeulen, N.; Sipe, J. E. Erratum: Third-order nonlinearity of graphene: Effects of phenomenological relaxation and finite temperature [Phys. Rev. B 91, 235320 (2015)]. *Phys. Rev. B: Condens. Matter Mater. Phys.* **2016**, *93*, 039904.
(13) Cheng, J. L.; Vermeulen, N.; Sipe, J. E. Numerical study of the optical nonlinearity of doped and gapped graphene: From weak to strong field excitation. *Phys. Rev. B: Condens. Matter Mater. Phys.* **2015**, *92*, 235307.
(14) Mikhailov, S. A. Quantum theory of the third-order nonlinear electrodynamic effects of graphene. *Phys. Rev. B: Condens. Matter Mater. Phys.* **2016**, *93*, 085403.
(15) Rostami, H.; Polini, M. Theory of third-harmonic generation in graphene: A diagrammatic approach. *Phys. Rev. B: Condens. Matter Mater. Phys.* **2016**, *93*, 161411.
(16) Margulis, V.; Muryumin, E.; Gaiduk, E. Frequency dependence of optical third-harmonic generation from doped graphene. *Phys. Lett. A* **2016**, *380*, 304−310.
(17) Hipolito, F.; Dimitrovski, D.; Pedersen, T. G. Iterative approach to arbitrary nonlinear optical response functions of graphene. *Phys. Rev. B: Condens. Matter Mater. Phys.* **2019**, *99*, 195407.
(18) Semnani, B.; Jago, R.; Safavi-Naeini, S.; Majedi, H.; Malic, E.; Tassin, P. Anomalous optical saturation of low-energy Dirac states in graphene and its implication for nonlinear optics. *2D Mater.* **2019**, *6*, 031003.
(19) Rostami, H.; Katsnelson, M. I.; Polini, M. Theory of plasmonic effects in nonlinear optics: The case of graphene. *Phys. Rev. B: Condens. Matter Mater. Phys.* **2017**, *95*, 035416.
(20) Avetissian, H. K.; Mkrtchian, G. F. Impact of electron-electron Coulomb interaction on the high harmonic generation process in graphene. *Phys. Rev. B: Condens. Matter Mater. Phys.* **2018**, *97*, 115454.
(21) Cheng, J. L.; Sipe, J. E.; Guo, C. Third harmonic generation of undoped graphene in Hartree-Fock approximation. *Phys. Rev. B: Condens. Matter Mater. Phys.* **2019**, *100*, 245433.
(22) Jafari, S. A. Nonlinear optical response in gapped graphene. *J. Phys.: Condens. Matter* **2012**, *24*, 205802.
(23) Cheng, J. L.; Guo, C. Nonlinear magneto-optic effects in doped graphene and in gapped graphene: A perturbative treatment. *Phys. Rev. B: Condens. Matter Mater. Phys.* **2018**, *97*, 125417.
(24) Cheng, J. L.; Sipe, J. E.; Wu, S. W.; Guo, C. Intraband divergences in third order optical response of 2D systems. *APL Photonics* **2019**, *4*, 034201.
(25) Young, S. M.; Zaheer, S.; Teo, J. C. Y.; Kane, C. L.; Mele, E. J.; Rappe, A. M. Dirac Semimetal in Three Dimensions. *Phys. Rev. Lett.* **2012**, *108*, 140405.
(26) Ma, J.; Deng, K.; Zheng, L.; Wu, S.; Liu, Z.; Zhou, S.; Sun, D. Experimental progress on layered topological semimetals. *2D Mater.* **2019**, *6*, 032001.
(27) Burkov, A. Weyl Metals. *Annu. Rev. Condens. Matter Phys.* **2018**, *9*, 359−378.
(28) Gao, H.; Venderbos, J. W.; Kim, Y.; Rappe, A. M. Topological Semimetals from First Principles. *Annu. Rev. Mater. Res.* **2019**, *49*, 153−183.
(29) Jia, S.; Xu, S.-Y.; Hasan, M. Z. Weyl semimetals, Fermi arcs and chiral anomalies. *Nat. Mater.* **2016**, *15*, 1140−1144.
(30) Rao, S. Weyl semi-metals: a short review. *arXiv:1603.02821* **2016**, na.
(31) Yan, B.; Felser, C. Topological Materials: Weyl Semimetals. *Annu. Rev. Condens. Matter Phys.* **2017**, *8*, 337−354.
(32) Yang, S. A. Dirac and Weyl Materials: Fundamental Aspects and Some Spintronics Applications. *SPIN* **2016**, *06*, 1640003.
(33) Moore, J. E. Optical properties of Weyl semimetals. *Natl. Sci. Rev.* **2019**, *6*, 206−208.
(34) Ma, Q.; Xu, S.-Y.; Chan, C.-K.; Zhang, C.-L.; Chang, G.; Lin, Y.; Xie, W.; Palacios, T.; Lin, H.; Jia, S.; Lee, P. A.; Jarillo-Herrero, P.; Gedik, N. Direct optical detection of Weyl fermion chirality in a topological semimetal. *Nat. Phys.* **2017**, *13*, 842−847.
(35) Ma, Q.; et al. Observation of the nonlinear Hall effect under time-reversal-symmetric conditions. *Nature* **2019**, *565*, 337−342.
(36) Chi, S.; Li, Z.; Yu, H.; Wang, G.; Wang, S.; Zhang, H.; Wang, J. Symmetrical broken and nonlinear response of Weyl semimetal TaAs influenced by the topological surface states and Weyl nodes. *Ann. Phys.* **2017**, *529*, 1600359.
(37) de Juan, F.; Grushin, A. G.; Morimoto, T.; Moore, J. E. Quantized circular photogalvanic effect in Weyl semimetals. *Nat. Commun.* **2017**, *8*, 15995.
(38) Sodemann, I.; Fu, L. Quantum Nonlinear Hall Effect Induced by Berry Curvature Dipole in Time-Reversal Invariant Materials. *Phys. Rev. Lett.* **2015**, *115*, 216806.
(39) Vazifeh, M. M.; Franz, M. Electromagnetic Response of Weyl Semimetals. *Phys. Rev. Lett.* **2013**, *111*, 027201.
(40) Yang, X.; Burch, K.; Ran, Y. Divergent bulk photovoltaic effect in Weyl semimetals. *arXiv:1712.09363 [cond-mat.mes-hall]* **2017**, na.
(41) Ma, J.; Gu, Q.; Liu, Y.; Lai, J.; Yu, P.; Zhuo, X.; Liu, Z.; Chen, J.-H.; Feng, J.; Sun, D. Nonlinear photoresponse of type-II Weyl semimetals. *Nat. Mater.* **2019**, *18*, 476−481.
(42) Ooi, K. J. A.; Ang, Y. S.; Zhai, Q.; Tan, D. T. H.; Ang, L. K.; Ong, C. K. Nonlinear plasmonics of three-dimensional Dirac semimetals. *APL Photonics* **2019**, *4*, 034402.
(43) Zhang, T.; Ooi, K. J. A.; Chen, W.; Ang, L. K.; Ang, Y. S. Optical Kerr effect and third harmonic generation in topological Dirac/Weyl semimetal. *Opt. Express* **2019**, *27*, 38270.
(44) Zhong, Y.; Feng, W.; Liu, Z.; Zhang, C.; Cao, J. C. Nonlinear optical conductivity of Weyl semimetals in the terahertz regime. *Phys. B* **2019**, *555*, 81−84.
(45) Ooi, K. J.; Ang, Y.; Zhai, Q.; Sun, X.; Xing, P.; Ong, C.; Ang, L.; Tan, D. T. Dirac terahertz plasmonics in two and three dimensions. *Opt. Commun.* **2020**, *462*, 125319.
(46) Sipe, J. E.; Ghahramani, E. Nonlinear optical response of semiconductors in the independent-particle approximation. *Phys. Rev. B: Condens. Matter Mater. Phys.* **1993**, *48*, 11705−11722.
(47) Taghizadeh, A.; Hipolito, F.; Pedersen, T. G. Linear and nonlinear optical response of crystals using length and velocity gauges: Effect of basis truncation. *Phys. Rev. B: Condens. Matter Mater. Phys.* **2017**, *96*, 195413.
(48) Almutairi, S.; Chen, Q.; Tokman, M.; Belyanin, A. Four-wave mixing in Weyl semimetals. *Phys. Rev. B: Condens. Matter Mater. Phys.* **2020**, *101*, 235156.
(49) Kotov, O. V.; Lozovik, Y. E. Dielectric response and novel electromagnetic modes in three-dimensional Dirac semimetal films. *Phys. Rev. B: Condens. Matter Mater. Phys.* **2016**, *93*, 235417.

https://dx.doi.org/10.1021/acsphotonics.0c00836
ACS Photonics 2020, 7, 2515−2526

(50) Sonowal, K.; Singh, A.; Agarwal, A. Giant optical activity and Kerr effect in type-I and type-II Weyl semimetals. *Phys. Rev. B: Condens. Matter Mater. Phys.* **2019**, *100*, 085436.
(51) Cheng, B.; Kanda, N.; Ikeda, T. N.; Matsuda, T.; Xia, P.; Schumann, T.; Stemmer, S.; Itatani, J.; Armitage, N. P.; Matsunaga, R. Efficient Terahertz Harmonic Generation with Coherent Acceleration of Electrons in the Dirac Semimetal Cd_3As_2. *Phys. Rev. Lett.* **2020**, *124*, 117402.
(52) Nair, R. R.; Blake, P.; Grigorenko, A. N.; Novoselov, K. S.; Booth, T. J.; Stauber, T.; Peres, N. M. R.; Geim, A. K. Fine Structure Constant Defines Visual Transparency of Graphene. *Science* **2008**, *320*, 1308.
(53) Crassee, I.; Sankar, R.; Lee, W.-L.; Akrap, A.; Orlita, M. 3D Dirac semimetal Cd_3As_2: A review of material properties. *Phys. Rev. Materials* **2018**, *2*, 120302.

https://dx.doi.org/10.1021/acsphotonics.0c00836
ACS Photonics 2020, 7, 2515−2526